

An improved measurement of $\eta' \rightarrow e^+e^-\omega$

M. Ablikim¹, M. N. Achasov^{4,c}, P. Adlarson⁸³, X. C. Ai⁸⁹, C. S. Akondi^{31A,31B}, R. Aliberti³⁹, A. Amoroso^{82A,82C}, Q. An^{79,65,†}, Y. H. An⁸⁹, Y. Bai⁶³, O. Bakina⁴⁰, H. R. Bao⁷¹, X. L. Bao⁵⁰, M. Barbagiovanni^{82C}, V. Batozskaya^{1,49}, K. Begzsuren³⁵, N. Berger³⁹, M. Berlowski⁴⁹, M. B. Bertani^{30A}, D. Bettoni^{31A}, F. Bianchi^{82A,82C}, E. Bianco^{82A,82C}, A. Bortone^{82A,82C}, I. Boyko⁴⁰, R. A. Briere⁵, A. Brueggemann⁷⁶, D. Cabiati^{82A,82C}, H. Cai⁸⁴, M. H. Cai^{42,k,l}, X. Cai^{1,65}, A. Calcaterra^{30A}, G. F. Cao^{1,71}, N. Cao^{1,71}, S. A. Cetin^{69A}, X. Y. Chai^{51,h}, J. F. Chang^{1,65}, T. T. Chang⁴⁸, G. R. Che⁴⁸, Y. Z. Che^{1,65,71}, C. H. Chen¹⁰, Chao Chen¹, G. Chen¹, H. S. Chen^{1,71}, H. Y. Chen²⁰, M. L. Chen^{1,65,71}, S. J. Chen⁴⁷, S. M. Chen⁶⁸, T. Chen^{1,71}, W. Chen⁵⁰, X. R. Chen^{34,71}, X. T. Chen^{1,71}, X. Y. Chen^{12,g}, Y. B. Chen^{1,65}, Y. Q. Chen¹⁶, Z. K. Chen⁶⁶, J. Cheng⁵⁰, L. N. Cheng⁴⁸, S. K. Choi¹¹, X. Chu^{12,g}, G. Cibinetto^{31A}, F. Cossio^{82C}, J. Cottee-Meldrum⁷⁰, H. L. Dai^{1,65}, J. P. Dai⁸⁷, X. C. Dai⁶⁸, A. Dbeyssi¹⁹, R. E. de Boer³, D. Dedovich⁴⁰, C. Q. Deng⁸⁰, Z. Y. Deng¹, A. Denig³⁹, I. Denisenko⁴⁰, M. Destefanis^{82A,82C}, F. De Mori^{82A,82C}, E. Di Fiore^{31A,31B}, X. X. Ding^{51,h}, Y. Ding⁴⁴, Y. X. Ding³², Yi. Ding³⁸, J. Dong^{1,65}, L. Y. Dong^{1,71}, M. Y. Dong^{1,65,71}, X. Y. Dong⁸⁴, Z. J. Dong⁶⁶, M. C. Du¹, S. X. Du⁸⁹, Shaoxu Du^{12,g}, X. L. Du^{12,g}, Y. Q. Du⁸⁴, Y. Y. Duan⁶¹, Z. H. Duan⁴⁷, P. Egorov^{40,a}, G. F. Fan⁴⁷, J. J. Fan²⁰, Y. H. Fan⁵⁰, J. Fang^{1,65}, Jin Fang⁶⁶, S. S. Fang^{1,71}, W. X. Fang¹, Y. Q. Fang^{1,65,†}, L. Fava^{82B,82C}, F. Feldbauer³, G. Felici^{30A}, C. Q. Feng^{79,65}, J. H. Feng¹⁶, L. Feng^{42,k,l}, Q. X. Feng^{42,k,l}, Y. T. Feng^{79,65}, M. Fritsch³, C. D. Fu¹, J. L. Fu⁷¹, Y. W. Fu^{1,71}, H. Gao⁷¹, Xu Gao³⁸, Y. Gao^{79,65}, Y. N. Gao^{51,h}, Y. Y. Gao³², Yunong Gao²⁰, Z. Gao⁴⁸, S. Garbolino^{82C}, I. Garzia^{31A,31B}, L. Ge⁶³, P. T. Ge²⁰, Z. W. Ge⁴⁷, C. Geng⁶⁶, E. M. Gersabeck⁷⁵, A. Gilman⁷⁷, K. Goetzen¹³, J. Gollub³, J. B. Gong^{1,71}, J. D. Gong³⁸, L. Gong⁴⁴, W. X. Gong^{1,65}, W. Gradl³⁹, S. Gramigna^{31A,31B}, M. Greco^{82A,82C}, M. D. Gu⁵⁶, M. H. Gu^{1,65}, C. Y. Guan^{1,71}, A. Q. Guo³⁴, H. Guo⁵⁵, J. N. Guo^{12,g}, L. B. Guo⁴⁶, M. J. Guo⁵⁵, R. P. Guo⁵⁴, X. H. Guo^{79,65}, Y. P. Guo^{12,g}, Z. Guo^{79,65}, A. Guskov^{40,a}, J. Gutierrez²⁹, J. Y. Han^{79,65}, T. T. Han¹, X. Han^{79,65}, F. Hanisch³, K. D. Hao^{79,65}, X. Q. Hao²⁰, F. A. Harris⁷², C. Z. He^{51,h}, K. K. He^{17,47}, K. L. He^{1,71}, F. H. Heinsius³, C. H. Heinz³⁹, Y. K. Heng^{1,65,71}, C. Herold⁶⁷, P. C. Hong³⁸, G. Y. Hou^{1,71}, X. T. Hou^{1,71}, Y. R. Hou⁷¹, Z. L. Hou¹, H. M. Hu^{1,71}, J. F. Hu^{62,j}, Q. P. Hu^{79,65}, S. L. Hu^{12,g}, T. Hu^{1,65,71}, Y. Hu¹, Y. X. Hu⁸⁴, Z. M. Hu⁶⁶, G. S. Huang^{79,65}, K. X. Huang⁶⁶, L. Q. Huang^{34,71}, P. Huang⁴⁷, X. T. Huang⁵⁵, Y. P. Huang¹, Y. S. Huang⁶⁶, T. Hussain⁸¹, N. Hüskens³⁹, N. in der Wiesche⁷⁶, J. Jackson²⁹, Q. Ji¹, Q. P. Ji²⁰, W. Ji^{1,71}, X. B. Ji^{1,71}, X. L. Ji^{1,65}, Y. Y. Ji¹, L. K. Jia⁷¹, X. Q. Jia⁵⁵, D. Jiang^{1,71}, H. B. Jiang⁸⁴, S. J. Jiang¹⁰, X. S. Jiang^{1,65,71}, Y. M. Jiang⁷¹, J. B. Jiao⁵⁵, J. K. Jiao³⁸, Z. Jiao²⁵, L. C. L. Jin¹, S. Jin⁴⁷, Y. Jin⁷³, M. Q. Jing⁵⁶, X. M. Jing⁷¹, T. Johansson⁸³, S. Kabana³⁶, X. L. Kang¹⁰, X. S. Kang⁴⁴, B. C. Ke⁸⁹, V. Khachatryan²⁹, A. Khoukaz⁷⁶, O. B. Kolcu^{69A}, B. Kopf³, L. Kröger⁷⁶, L. Krümmel³, Y. Y. Kuang⁸⁰, M. Kuessner³, X. Kui^{1,71}, N. Kumar²⁸, A. Kupsc^{49,83}, W. Kühn⁴¹, Q. Lan⁸⁰, W. N. Lan²⁰, T. T. Lei^{79,65}, M. Lellmann³⁹, T. Lenz³⁹, C. Li⁵², C. H. Li⁴⁶, C. K. Li⁴⁸, Chunkai Li²¹, Cong Li⁴⁸, D. M. Li⁸⁹, F. Li^{1,65}, G. Li¹, H. B. Li^{1,71}, H. J. Li²⁰, H. L. Li⁸⁹, H. N. Li^{62,j}, H. P. Li⁴⁸, Hui Li⁴⁸, J. N. Li³², J. S. Li⁶⁶, J. W. Li⁵⁵, K. Li¹, K. L. Li^{42,k,l}, L. J. Li^{1,71}, L. K. Li²⁶, Lei Li⁵³, M. H. Li⁴⁸, M. R. Li^{1,71}, M. T. Li⁵⁵, P. L. Li⁷¹, P. R. Li^{42,k,l}, Q. M. Li^{1,71}, Q. X. Li⁵⁵, R. Li^{18,34}, S. Li⁸⁹, S. X. Li⁸⁹, S. Y. Li⁸⁹, Shanshan Li^{27,i}, T. Li⁵⁵, T. Y. Li⁴⁸, W. D. Li^{1,71}, W. G. Li^{1,†}, X. Li^{1,71}, X. H. Li^{79,65}, X. K. Li^{51,h}, X. L. Li⁵⁵, X. Y. Li^{1,9}, X. Z. Li⁶⁶, Y. Li²⁰, Y. H. Li⁴⁸, Y. B. Li⁸⁵, Y. C. Li⁶⁶, Y. G. Li⁷¹, Y. P. Li³⁸, Z. H. Li⁴², Z. J. Li⁶⁶, Z. L. Li⁸⁹, Z. X. Li⁴⁸, Z. Y. Li⁸⁷, C. Liang⁴⁷, H. Liang^{79,65}, Y. F. Liang⁶⁰, Y. T. Liang^{34,71}, Z. Z. Liang⁶⁶, G. R. Liao¹⁴, L. B. Liao⁶⁶, M. H. Liao⁶⁶, Y. P. Liao^{1,71}, J. Libby²⁸, A. Limphirat⁶⁷, C. C. Lin⁶¹, C. X. Lin³⁴, D. X. Lin^{34,71}, T. Lin¹, B. J. Liu¹, B. X. Liu⁸⁴, C. Liu³⁸, C. X. Liu¹, F. Liu¹, F. H. Liu⁵⁹, Feng Liu⁶, G. M. Liu^{62,j}, H. Liu^{42,k,l}, H. B. Liu¹⁵, H. M. Liu^{1,71}, Huihui Liu²², J. B. Liu^{79,65}, J. J. Liu²¹, K. Liu^{42,k,l}, K. Y. Liu^{43,44}, Ke Liu²³, Kun Liu⁸⁰, L. Liu⁴², L. C. Liu⁴⁸, Lu Liu⁴⁸, M. H. Liu³⁸, P. L. Liu⁵⁵, Q. Liu⁷¹, S. B. Liu^{79,65}, T. Liu¹, W. M. Liu^{79,65}, W. T. Liu⁴³, X. Liu^{42,k,l}, X. K. Liu^{42,k,l}, X. L. Liu^{12,g}, X. P. Liu^{12,g}, X. T. Liu²¹, X. Y. Liu⁸⁴, Y. Liu^{42,k,l}, Y. B. Liu⁴⁸, Yi Liu⁸⁹, Z. A. Liu^{1,65,71}, Z. D. Liu⁸⁵, Z. L. Liu⁸⁰, Z. Q. Liu⁵⁵, Z. X. Liu¹, Z. Y. Liu⁴², X. C. Lou^{1,65,71}, H. J. Lu²⁵, J. G. Lu^{1,65}, X. L. Lu¹⁶, Y. Lu⁷, Y. H. Lu^{1,71}, Y. P. Lu^{1,65}, Z. H. Lu^{1,71}, C. L. Luo⁴⁶, J. R. Luo⁶⁶, J. S. Luo^{1,71}, M. X. Luo⁸⁸, T. Luo^{12,g}, X. L. Luo^{1,65}, Z. Y. Lv²³, X. R. Lyu^{71,o}, Y. F. Lyu⁴⁸, Y. H. Lyu⁸⁹, F. C. Ma⁴⁴, H. L. Ma¹, Heng Ma^{27,i}, J. L. Ma^{1,71}, L. L. Ma⁵⁵, L. R. Ma⁷³, Q. M. Ma¹, R. Q. Ma^{1,71}, R. Y. Ma²⁰, T. Ma^{79,65}, X. T. Ma^{1,71}, X. Y. Ma^{1,65}, Y. M. Ma³⁴, F. E. Maas¹⁹, I. MacKay⁷⁷, M. Maggiora^{82A,82C}, S. Maity³⁴, S. Malde⁷⁷, Q. A. Malik⁸¹, H. X. Mao^{42,k,l}, Y. J. Mao^{51,h}, Z. P. Mao¹, S. Marcello^{82A,82C}, A. Marshall⁷⁰, F. M. Melendi^{31A,31B}, Y. H. Meng⁷¹, Z. X. Meng⁷³, G. Mezzadri^{31A}, H. Miao^{1,71}, T. J. Min⁴⁷, R. E. Mitchell²⁹, X. H. Mo^{1,65,71}, B. Moses²⁹, N. Yu. Muchnoi^{4,c}, J. Muskalla³⁹, Y. Nefedov⁴⁰, F. Nerling^{19,e}, H. Neuwirth⁷⁶, Z. Ning^{1,65}, S. Nisar³³, Q. L. Niu^{42,k,l}, W. D. Niu^{12,g}, Y. Niu⁵⁵, C. Normand⁷⁰, S. L. Olsen^{11,71}, Q. Ouyang^{1,65,71}, I. V. Ovtin⁴, S. Pacetti^{30B,30C}, Y. Pan⁶³, A. Pathak¹¹, Y. P. Pei^{79,65}, M. Pelizaeus³, G. L. Peng^{79,65}, H. P. Peng^{79,65}, X. J. Peng^{42,k,l}, Y. Y. Peng^{42,k,l}, K. Peters^{13,e}, K. Petridis⁷⁰, J. L. Ping⁴⁶, R. G. Ping^{1,71}, S. Plura³⁹, V. Prasad³⁸, L. Pöpping³, F. Z. Qi¹, H. R. Qi⁶⁸, M. Qi⁴⁷, S. Qian^{1,65}, W. B. Qian⁷¹, C. F. Qiao⁷¹, J. H. Qiao²⁰, J. J. Qin⁸⁰, J. L. Qin⁶¹, L. Q. Qin¹⁴, L. Y. Qin^{79,65}, P. B. Qin⁸⁰, X. P. Qin⁴³, X. S. Qin⁵⁵, Z. H. Qin^{1,65}, J. F. Qiu¹, Z. H. Qu⁸⁰, J. Rademacker⁷⁰, K. Ravindran⁷⁴, C. F. Redmer³⁹, A. Rivetti^{82C}, M. Rolo^{82C}, G. Rong^{1,71}, S. S. Rong^{1,71}, F. Rosini^{30B,30C}, Ch. Rosner¹⁹, M. Q. Ruan^{1,65}

N. Salone^{49,q} , A. Sarantsev^{40,d} , Y. Schelhaas³⁹ , M. Schernau³⁶ , K. Schoenning⁸³ , M. Scodreggio^{31A} ,
W. Shan²⁶ , X. Y. Shan^{79,65} , Z. J. Shang^{42,k,l} , J. F. Shangguan¹⁷ , L. G. Shao^{1,71} , M. Shao^{79,65} ,
C. P. Shen^{12,g} , H. F. Shen^{1,9} , W. H. Shen⁷¹ , X. Y. Shen^{1,71} , B. A. Shi⁷¹ , Ch. Y. Shi^{87,b} , H. Shi^{79,65} ,
J. L. Shi^{8,p} , J. Y. Shi¹ , M. H. Shi⁸⁹ , S. Y. Shi⁸⁰ , X. Shi^{1,65} , H. L. Song^{79,65} , J. J. Song²⁰ , M. H. Song⁴² ,
T. Z. Song⁶⁶ , W. M. Song³⁸ , Y. X. Song^{51,h,m} , Zirong Song^{27,i} , S. Sosio^{82A,82C} , S. Spataro^{82A,82C} ,
S. Stansilau⁷⁷ , F. Stieler³⁹ , M. Stolte³ , S. S. Su⁴⁴ , G. B. Sun⁸⁴ , G. X. Sun¹ , H. Sun⁷¹ , H. K. Sun¹ ,
J. F. Sun²⁰ , K. Sun⁶⁸ , L. Sun⁸⁴ , R. Sun⁷⁹ , S. S. Sun^{1,71} , T. Sun^{57,f} , W. Y. Sun⁵⁶ , Y. C. Sun⁸⁴ ,
Y. H. Sun³² , Y. J. Sun^{79,65} , Y. Z. Sun¹ , Z. Q. Sun^{1,71} , Z. T. Sun⁵⁵ , H. Tabaharizato¹ , C. J. Tang⁶⁰ ,
G. Y. Tang¹ , J. J. Tang⁶⁶ , L. F. Tang⁴³ , Y. A. Tang⁸⁴ , Z. H. Tang^{1,71} , L. Y. Tao⁸⁰ ,
M. Tat⁷⁷ , J. X. Teng^{79,65} , J. Y. Tian^{79,65} , W. H. Tian⁶⁶ , Y. Tian³⁴ , Z. F. Tian⁸⁴ , K. Yu. Todyshev⁴ ,
I. Uman^{69B} , E. van der Smagt³ , B. Wang⁶⁶ , Bin Wang¹ , Bo Wang^{79,65} , C. Wang^{42,k,l} , Chao Wang²⁰ ,
Cong Wang²³ , D. Y. Wang^{51,h} , F. K. Wang⁶⁶ , H. J. Wang^{42,k,l} , H. R. Wang⁸⁶ , J. Wang¹⁰ , J. J. Wang⁸⁴ ,
J. P. Wang³⁷ , K. Wang^{1,65} , L. L. Wang¹ , L. W. Wang³⁸ , M. Wang⁵⁵ , Mi Wang^{79,65} , N. Y. Wang⁷¹ ,
P. Wang²¹ , S. Wang^{42,k,l} , Shun Wang⁶⁴ , T. Wang^{12,g} , W. Wang⁶⁶ , W. P. Wang³⁹ , X. F. Wang^{42,k,l} ,
X. L. Wang^{12,g} , X. N. Wang^{1,71} , Xin Wang^{27,i} , Y. Wang¹ , Y. D. Wang⁵⁰ , Y. F. Wang^{1,9,71} ,
Y. H. Wang^{42,k,l} , Y. J. Wang^{79,65} , Y. L. Wang²⁰ , Y. N. Wang⁵⁰ , Yanping Wang⁸⁴ , Yaqian Wang¹⁸ ,
Yi Wang⁶⁸ , Yuan Wang^{18,34} , Z. Wang^{1,65} , Z. L. Wang² , Z. Q. Wang^{12,g} , Z. Y. Wang^{1,71} , Zhi Wang⁴⁸ ,
Ziyi Wang⁷¹ , D. Wei⁴⁸ , D. H. Wei¹⁴ , D. J. Wei⁷³ , H. R. Wei⁴⁸ , F. Weidner⁷⁶ , H. R. Wen³⁴ , S. P. Wen¹ ,
U. Wiedner³ , G. Wilkinson⁷⁷ , M. Wolke⁸³ , J. F. Wu^{1,9} , L. H. Wu¹ , L. J. Wu²⁰ , Lianjie Wu²⁰ , S. G. Wu^{1,71} ,
S. M. Wu⁷¹ , X. W. Wu⁸⁰ , Z. Wu^{1,65} , H. L. Xia^{79,65} , L. Xia^{79,65} , B. H. Xiang^{1,71} , D. Xiao^{42,k,l} ,
G. Y. Xiao⁴⁷ , H. Xiao⁸⁰ , Y. L. Xiao^{12,g} , Z. J. Xiao⁴⁶ , C. Xie⁴⁷ , K. J. Xie^{1,71} , Y. Xie⁵⁵ , Y. G. Xie^{1,65} ,
Y. H. Xie⁶ , Z. P. Xie^{79,65} , T. Y. Xing^{1,71} , D. B. Xiong¹ , G. F. Xu¹ , H. Y. Xu² , Q. J. Xu¹⁷ , Q. N. Xu³² ,
T. D. Xu⁸⁰ , X. P. Xu⁶¹ , Y. Xu^{12,g} , Y. C. Xu⁸⁶ , Z. S. Xu⁷¹ , F. Yan²⁴ , L. Yan^{12,g} , W. B. Yan^{79,65} ,
W. C. Yan⁸⁹ , W. H. Yan⁶ , W. P. Yan²⁰ , X. Q. Yan^{12,g} , Y. Y. Yan^{57,f} , H. J. Yang³⁸ , H. L. Yang⁴⁸ ,
H. X. Yang¹ , J. H. Yang⁴⁷ , R. J. Yang²⁰ , X. Y. Yang⁷³ , Y. Yang^{12,g} , Y. G. Yang⁵⁶ , Y. H. Yang⁴⁸ ,
Y. M. Yang⁸⁹ , Y. Q. Yang¹⁰ , Y. Z. Yang²⁰ , Youhua Yang⁴⁷ , Z. Y. Yang⁸⁰ , W. J. Yao⁶ , Z. P. Yao⁵⁵ ,
M. Ye^{1,65} , M. H. Ye^{9,†} , Z. J. Ye^{62,j} , K. Yi⁴⁶ , Junhao Yin⁴⁸ , Z. Y. You⁶⁶ , B. X. Yu^{1,65,71} , C. X. Yu⁴⁸ ,
G. Yu¹³ , J. S. Yu^{27,i} , L. W. Yu^{12,g} , T. Yu⁸⁰ , X. D. Yu^{51,h} , Y. C. Yu⁸⁹ , Yongchao Yu⁴² , C. Z. Yuan^{1,71} ,
H. Yuan^{1,71} , J. Yuan³⁸ , Jie Yuan⁵⁰ , L. Yuan² , M. K. Yuan^{12,g} , S. H. Yuan⁸⁰ , Y. Yuan^{1,71} , C. X. Yue⁴³ ,
Ying Yue²⁰ , A. A. Zafar⁸¹ , F. R. Zeng⁵⁵ , S. H. Zeng⁷⁰ , X. Zeng^{12,g} , Y. J. Zeng^{1,71} , Yujie Zeng⁶⁶ ,
Y. C. Zhai⁵⁵ , Y. H. Zhan⁶⁶ , B. L. Zhang^{1,71} , B. X. Zhang^{1,†} , D. H. Zhang⁴⁸ , G. Y. Zhang²⁰ ,
Gengyuan Zhang^{1,71} , H. Zhang^{79,65} , H. C. Zhang^{1,65,71} , H. H. Zhang⁶⁶ , H. Q. Zhang^{1,65,71} , H. R. Zhang^{79,65} ,
H. Y. Zhang^{1,65} , Han Zhang⁸⁹ , J. Zhang⁶⁶ , J. J. Zhang⁵⁸ , J. L. Zhang²¹ , J. Q. Zhang⁴⁶ , J. S. Zhang^{12,g} ,
J. W. Zhang^{1,65,71} , J. X. Zhang^{42,k,l} , J. Y. Zhang¹ , J. Z. Zhang^{1,71} , Jianyu Zhang⁷¹ , Jin Zhang⁵³ ,
Jiyuan Zhang^{12,g} , L. M. Zhang⁶⁸ , Lei Zhang⁴⁷ , N. Zhang³⁸ , P. Zhang^{1,9} , Q. Zhang²⁰ , Q. Y. Zhang³⁸ ,
Q. Z. Zhang⁷¹ , R. Y. Zhang^{42,k,l} , S. H. Zhang^{1,71} , S. N. Zhang⁷⁷ , Shulei Zhang^{27,i} , X. M. Zhang¹ ,
X. Y. Zhang⁵⁵ , Y. T. Zhang⁸⁹ , Y. H. Zhang^{1,65} , Y. P. Zhang^{79,65} , Yao Zhang¹ , Yu Zhang⁸⁰ , Yu Zhang⁶⁶ ,
Z. Zhang³⁴ , Z. D. Zhang¹ , Z. H. Zhang¹ , Z. L. Zhang³⁸ , Z. X. Zhang²⁰ , Z. Y. Zhang⁸⁴ , Zh. Zh. Zhang²⁰ ,
Zhilong Zhang⁶¹ , Ziyang Zhang⁵⁰ , Ziyu Zhang⁴⁸ , G. Zhao¹ , J.-P. Zhao⁷¹ , J. Y. Zhao^{1,71} , J. Z. Zhao^{1,65} ,
L. Zhao¹ , Lei Zhao^{79,65} , M. G. Zhao⁴⁸ , R. P. Zhao⁷¹ , S. J. Zhao⁸⁹ , Y. B. Zhao^{1,65} , Y. L. Zhao⁶¹ ,
Y. P. Zhao⁵⁰ , Y. X. Zhao^{34,71} , Z. G. Zhao^{79,65} , A. Zhemchugov^{40,a} , B. Zheng⁸⁰ , B. M. Zheng³⁸ ,
J. P. Zheng^{1,65} , W. J. Zheng^{1,71} , W. Q. Zheng¹⁰ , X. R. Zheng²⁰

- ¹⁶ Guangxi University of Science and Technology, Liuzhou 545006, People's Republic of China
- ¹⁷ Hangzhou Normal University, Hangzhou 310036, People's Republic of China
- ¹⁸ Hebei University, Baoding 071002, People's Republic of China
- ¹⁹ Helmholtz Institute Mainz, Staudinger Weg 18, D-55099 Mainz, Germany
- ²⁰ Henan Normal University, Xinxiang 453007, People's Republic of China
- ²¹ Henan University, Kaifeng 475004, People's Republic of China
- ²² Henan University of Science and Technology, Luoyang 471003, People's Republic of China
- ²³ Henan University of Technology, Zhengzhou 450001, People's Republic of China
- ²⁴ Hengyang Normal University, Hengyang 421001, People's Republic of China
- ²⁵ Huangshan College, Huangshan 245000, People's Republic of China
- ²⁶ Hunan Normal University, Changsha 410081, People's Republic of China
- ²⁷ Hunan University, Changsha 410082, People's Republic of China
- ²⁸ Indian Institute of Technology Madras, Chennai 600036, India
- ²⁹ Indiana University, Bloomington, Indiana 47405, USA
- ³⁰ INFN Laboratori Nazionali di Frascati, (A)INFN Laboratori Nazionali di Frascati, I-00044, Frascati, Italy; (B)INFN Sezione di Perugia, I-06100, Perugia, Italy; (C)University of Perugia, I-06100, Perugia, Italy
- ³¹ INFN Sezione di Ferrara, (A)INFN Sezione di Ferrara, I-44122, Ferrara, Italy; (B)University of Ferrara, I-44122, Ferrara, Italy
- ³² Inner Mongolia University, Hohhot 010021, People's Republic of China
- ³³ Institute of Business Administration, University Road, Karachi, 75270 Pakistan
- ³⁴ Institute of Modern Physics, Lanzhou 730000, People's Republic of China
- ³⁵ Institute of Physics and Technology, Mongolian Academy of Sciences, Peace Avenue 54B, Ulaanbaatar 13330, Mongolia
- ³⁶ Instituto de Alta Investigación, Universidad de Tarapacá, Casilla 7D, Arica 1000000, Chile
- ³⁷ Jiangsu Ocean University, Lianyungang 222000, People's Republic of China
- ³⁸ Jilin University, Changchun 130012, People's Republic of China
- ³⁹ Johannes Gutenberg University of Mainz, Johann-Joachim-Becher-Weg 45, D-55099 Mainz, Germany
- ⁴⁰ Joint Institute for Nuclear Research, 141980 Dubna, Moscow region, Russia
- ⁴¹ Justus-Liebig-Universität Giessen, II. Physikalisches Institut, Heinrich-Buff-Ring 16, D-35392 Giessen, Germany
- ⁴² Lanzhou University, Lanzhou 730000, People's Republic of China
- ⁴³ Liaoning Normal University, Dalian 116029, People's Republic of China
- ⁴⁴ Liaoning University, Shenyang 110036, People's Republic of China
- ⁴⁵ Longyan University, Longyan 364000, People's Republic of China
- ⁴⁶ Nanjing Normal University, Nanjing 210023, People's Republic of China
- ⁴⁷ Nanjing University, Nanjing 210093, People's Republic of China
- ⁴⁸ Nankai University, Tianjin 300071, People's Republic of China
- ⁴⁹ National Centre for Nuclear Research, Warsaw 02-093, Poland
- ⁵⁰ North China Electric Power University, Beijing 102206, People's Republic of China
- ⁵¹ Peking University, Beijing 100871, People's Republic of China
- ⁵² Qufu Normal University, Qufu 273165, People's Republic of China
- ⁵³ Renmin University of China, Beijing 100872, People's Republic of China
- ⁵⁴ Shandong Normal University, Jinan 250014, People's Republic of China
- ⁵⁵ Shandong University, Jinan 250100, People's Republic of China
- ⁵⁶ Shandong University of Technology, Zibo 255000, People's Republic of China
- ⁵⁷ Shanghai Jiao Tong University, Shanghai 200240, People's Republic of China
- ⁵⁸ Shanxi Normal University, Linfen 041004, People's Republic of China
- ⁵⁹ Shanxi University, Taiyuan 030006, People's Republic of China
- ⁶⁰ Sichuan University, Chengdu 610064, People's Republic of China
- ⁶¹ Soochow University, Suzhou 215006, People's Republic of China
- ⁶² South China Normal University, Guangzhou 510006, People's Republic of China
- ⁶³ Southeast University, Nanjing 211100, People's Republic of China
- ⁶⁴ Southwest University of Science and Technology, Mianyang 621010, People's Republic of China
- ⁶⁵ State Key Laboratory of Particle Detection and Electronics, Beijing 100049, Hefei 230026, People's Republic of China
- ⁶⁶ Sun Yat-Sen University, Guangzhou 510275, People's Republic of China
- ⁶⁷ Suranaree University of Technology, University Avenue 111, Nakhon Ratchasima 30000, Thailand
- ⁶⁸ Tsinghua University, Beijing 100084, People's Republic of China
- ⁶⁹ Turkish Accelerator Center Particle Factory Group, (A)Istinye University, 34010, Istanbul, Turkey; (B)Near East University, Nicosia, North Cyprus, 99138, Mersin 10, Turkey
- ⁷⁰ University of Bristol, H H Wills Physics Laboratory, Tyndall Avenue, Bristol, BS8 1TL, United Kingdom
- ⁷¹ University of Chinese Academy of Sciences, Beijing 100049, People's Republic of China
- ⁷² University of Hawaii, Honolulu, Hawaii 96822, USA
- ⁷³ University of Jinan, Jinan 250022, People's Republic of China
- ⁷⁴ University of La Serena, Av. Raúl Bitrán 1305, La Serena, Chile
- ⁷⁵ University of Manchester, Oxford Road, Manchester, M13 9PL, United Kingdom
- ⁷⁶ University of Muenster, Wilhelm-Klemm-Strasse 9, 48149 Muenster, Germany

⁷⁷ University of Oxford, Keble Road, Oxford OX13RH, United Kingdom

⁷⁸ University of Science and Technology Liaoning, Anshan 114051, People's Republic of China

⁷⁹ University of Science and Technology of China, Hefei 230026, People's Republic of China

⁸⁰ University of South China, Hengyang 421001, People's Republic of China

⁸¹ University of the Punjab, Lahore-54590, Pakistan

⁸² University of Turin and INFN, (A)University of Turin, I-10125, Turin, Italy; (B)University of Eastern Piedmont, I-15121, Alessandria, Italy; (C)INFN, I-10125, Turin, Italy

⁸³ Uppsala University, Box 516, SE-75120 Uppsala, Sweden

⁸⁴ Wuhan University, Wuhan 430072, People's Republic of China

⁸⁵ Xi'an Jiaotong University, No.28 Xianning West Road, Xi'an, Shaanxi 710049, P.R. China

⁸⁶ Yantai University, Yantai 264005, People's Republic of China

⁸⁷ Yunnan University, Kunming 650500, People's Republic of China

⁸⁸ Zhejiang University, Hangzhou 310027, People's Republic of China

⁸⁹ Zhengzhou University, Zhengzhou 450001, People's Republic of China

[†] Deceased

^a Also at the Moscow Institute of Physics and Technology, Moscow 141700, Russia

^b Also at the Functional Electronics Laboratory, Tomsk State University, Tomsk, 634050, Russia

^c Also at the Novosibirsk State University, Novosibirsk, 630090, Russia

^d Also at the NRC "Kurchatov Institute", PNPI, 188300, Gatchina, Russia

^e Also at Goethe University Frankfurt, 60323 Frankfurt am Main, Germany

^f Also at Key Laboratory for Particle Physics, Astrophysics and Cosmology, Ministry of Education; Shanghai Key Laboratory for Particle Physics and Cosmology; Institute of Nuclear and Particle Physics, Shanghai 200240, People's Republic of China

^g Also at Key Laboratory of Nuclear Physics and Ion-beam Application (MOE) and Institute of Modern Physics, Fudan University, Shanghai 200443, People's Republic of China

^h Also at State Key Laboratory of Nuclear Physics and Technology, Peking University, Beijing 100871, People's Republic of China

ⁱ Also at School of Physics and Electronics, Hunan University, Changsha 410082, China

^j Also at Guangdong Provincial Key Laboratory of Nuclear Science, Institute of Quantum Matter, South China Normal University, Guangzhou 510006, China

^k Also at MOE Frontiers Science Center for Rare Isotopes, Lanzhou University, Lanzhou 730000, People's Republic of China

^l Also at Lanzhou Center for Theoretical Physics, Lanzhou University, Lanzhou 730000, People's Republic of China

^m Also at Ecole Polytechnique Federale de Lausanne (EPFL), CH-1015 Lausanne, Switzerland

ⁿ Also at Helmholtz Institute Mainz, Staudinger Weg 18, D-55099 Mainz, Germany

^o Also at Hangzhou Institute for Advanced Study, University of Chinese Academy of Sciences, Hangzhou 310024, China

^p Also at Applied Nuclear Technology in Geosciences Key Laboratory of Sichuan Province, Chengdu University of Technology, Chengdu 610059, People's Republic of China

^q Currently at University of Silesia in Katowice, Institute of Physics, 75 Pulku Piechoty 1, 41-500 Chorzow, Poland

(Dated: March 10, 2026)

Using a sample of $(10087 \pm 44) \times 10^6$ J/ψ events collected with the BESIII detector, an improved measurement of the decay $\eta' \rightarrow e^+e^-\omega$, with $\omega \rightarrow \pi^+\pi^-\pi^0$ and $\pi^0 \rightarrow \gamma\gamma$ is performed. The branching fraction is determined to be $\mathcal{B}(\eta' \rightarrow e^+e^-\omega) = (1.79 \pm 0.09 \pm 0.12) \times 10^{-4}$, where the first uncertainty is statistical and the second is systematic. This result is consistent with the previous measurement and is obtained with significantly improved precision. Furthermore, the first measurement of the transition form factor cutoff parameter for this decay is reported, with $\Lambda^{-1} = (2.92 \pm 0.83 \pm 0.15) \text{ GeV}^{-1}$. These measurements provide valuable input for understanding the internal structure of the η' meson and testing theoretical models.

I. INTRODUCTION

The pseudoscalar meson η' , discovered in 1964 [1, 2], remains a subject of significant interest because its decay properties serve as a probe of meson internal structure and a testing ground for low-energy quantum chromodynamics (QCD). Its decay properties can be classified into two main categories. Hadronic decays, such as $\eta' \rightarrow \eta\pi\pi$, are dominant and governed by isospin conservation. Radiative decays into vector mesons, such as $\eta' \rightarrow \rho^0\gamma$ and $\eta' \rightarrow \omega\gamma$, serve as a testing ground for model-dependent approaches, including Vector Meson Dominance (VMD) and chiral perturbation theory.

Decays of the form $\eta' \rightarrow Ve^+e^-$ (where V denotes a vector meson) are particularly insightful, as they proceed via a virtual photon $\eta' \rightarrow V\gamma^* \rightarrow Ve^+e^-$. The invariant mass spectrum of the e^+e^- pair provides direct access to the η' transition form factor (TFF). The TFF encapsulates the meson's internal structure and its dependence on the momentum transfer, q^2 , making it a valuable tool for phenomenological studies. A decay of similar nature, $\eta' \rightarrow \pi^+\pi^-e^+e^-$, has been previously measured [3] and agrees with the theoretical predictions [4].

The branching fraction(BF) for $\eta' \rightarrow e^+e^-\omega$ was previously measured by BESIII to be $\mathcal{B}(\eta' \rightarrow e^+e^-\omega) = (1.97 \pm 0.34 \text{ (stat.)} \pm 0.17 \text{ (syst.)}) \times 10^{-4}$ using $(1310.6 \pm$

$7.2) \times 10^6$ J/ψ events [5].

In this work, we present an improved analysis of the decay $\eta' \rightarrow e^+e^-\omega$, with $\omega \rightarrow \pi^+\pi^-\pi^0$ and $\pi^0 \rightarrow \gamma\gamma$, using the process $J/\psi \rightarrow \gamma\eta'$. The analysis utilizes a significantly larger data sample of $(10087 \pm 44) \times 10^6$ J/ψ events [6]. We report a more precise measurement of the BF and, for the first time, a measurement of the TFF parameter for this decay channel.

II. BESIII DETECTOR AND MONTE CARLO SIMULATION

The BESIII detector [7] records symmetric e^+e^- collisions provided by the BEPCII storage ring [8] in the center-of-mass energy range from 1.84 to 4.95 GeV, with a peak luminosity of 1.1×10^{33} $\text{cm}^{-2}\text{s}^{-1}$ achieved at $\sqrt{s} = 3.773$ GeV. The BESIII detector has accumulated the world's largest sample of J/ψ events in this energy region, which provides the foundation for this high-precision study [9]. The cylindrical core of the BESIII detector covers 93% of the full solid angle and consists of a helium-based multilayer drift chamber (MDC), a plastic scintillator time-of-flight system (TOF), and a CsI (Tl) electromagnetic calorimeter (EMC), which are all enclosed in a superconducting solenoidal magnet providing a 1.0 T magnetic field. The solenoid's magnetic field was 0.9 T during the data-taking period in 2012, which accounts for approximately 10% of the total J/ψ data sample. The solenoid is supported by an octagonal flux-return yoke with resistive plate counter muon identification modules interleaved with steel. The charged-particle momentum resolution at 1 GeV/ c is 0.5%, and the dE/dx resolution is 6% for electrons from Bhabha scattering. The EMC measures photon energies with a resolution of 2.5% (5%) at 1 GeV in the barrel (end cap) region. The time resolution in the TOF barrel region is 68 ps, while that in the end cap region was 110 ps. The end cap TOF system was upgraded in 2015 using multi-gap resistive plate chamber technology, providing a time resolution of 60 ps [10], which benefits 87% of the data used in this analysis.

Simulated data samples produced with a GEANT4-based [11] Monte Carlo (MC) package, including the geometric description of the BESIII detector and the detector response, are used to determine detection efficiencies and to estimate backgrounds. The simulation models the beam energy spread and initial state radiation (ISR) in the e^+e^- annihilations with the generator KKMC [12, 13]. All particle decays are modeled with EVTGEN [14, 15] using BFs either taken from the Particle Data Group (PDG) [16], when available, or otherwise estimated with LUNDCHARM [17, 18]. Final state radiation (FSR) from charged final state particles is incorporated using the PHOTOS package [19].

The decay chain of the signal process $J/\psi \rightarrow \gamma\eta'$, $\eta' \rightarrow e^+e^-\omega$, $\omega \rightarrow \pi^+\pi^-\pi^0$, and $\pi^0 \rightarrow \gamma\gamma$ containing 5 million events are produced. In this analysis, the simu-

lation of the $\eta' \rightarrow e^+e^-\omega$ process uses the parameters of the TFF, which is parametrized following the approach in Ref. [20]. Within the effective meson theory framework, the squared amplitude for the decay $\eta' \rightarrow e^+e^-\omega$ is given by

$$|\mathcal{A}_{\eta' \rightarrow e^+e^-\omega}|^2 = \frac{2^6 \pi^2 M_{\eta'}^3 \alpha \Gamma_{\eta' \rightarrow \gamma\omega}}{(M_{\eta'}^2 - M_\omega^2)^3} |F(q^2)|^2 \cdot \frac{(M_{\eta'}^2 - q^2 - M_\omega^2)^2 - 4M_\omega^2 q^2}{q^2} (2 - \beta^2 \sin^2 \theta), \quad (1)$$

where $\alpha = 1/137$, $q^2 = (q_{e^+} + q_{e^-})^2$, q_{e^\pm} denotes the four-momentum of e^\pm ; $\Gamma_{\eta' \rightarrow \gamma\omega}$ denotes the decay width of $\eta' \rightarrow \gamma\omega$ and is quoted from the PDG [16]; $M_{\eta'}$ and M_ω are the masses of the η' and ω , respectively, quoted from the PDG [16]; $\beta = \sqrt{1 - \frac{4M_{e^\pm}^2}{q^2}}$; and θ is the polar angle of q_{e^\pm} in the e^+e^- rest frame with respect to the direction of the flight of the $q_{e^+} + q_{e^-}$ in the pseudoscalar rest frame. In the VMD model, the interactions between a virtual photon and hadrons are assumed to be dominated by a superposition of neutral vector meson states. The TFF can be parametrized as [21]

$$F(q^2) = N \sum \frac{g_{\eta'\gamma\omega}}{2g_{\omega\gamma}} \frac{m_\omega^2}{m_\omega^2 - q^2 - i\Gamma_\omega m_\omega}, \quad (2)$$

where N is a normalization constant ensuring $F(0) = 1$; m_ω and Γ_ω are the mass and width of ω , and $g_{\eta'\gamma\omega}$ and $g_{\omega\gamma}$ correspond to the respective coupling constants. When there is a single dominant vector meson, the single-pole approximation is often used:

$$F(q^2) = \frac{1}{1 - q^2/\Lambda^2}. \quad (3)$$

Here, the single parameter Λ can be experimentally determined from the slope of the TFF, defined as:

$$\text{slope} \equiv \left. \frac{dF}{dq^2} \right|_{q^2=0} = \frac{1}{\Lambda^2}. \quad (4)$$

III. EVENT SELECTION AND BACKGROUND ANALYSIS

Charged tracks with a polar angle $|\cos\theta| \leq 0.93$ and passing the interaction point within ± 20 cm along the beam direction and within ± 2 cm in the plane perpendicular to the beam are accepted. Photon candidates are required to have an energy deposition above 25 MeV in the barrel EMC ($|\cos\theta| < 0.8$) or 50 MeV in the end cap EMC ($0.86 < |\cos\theta| < 0.92$). To exclude showers from charged particles, the opening angle between the shower direction and the charged tracks extrapolated to the EMC must be greater than 10 degrees. A requirement on the EMC timing ($0 \leq t \leq 700$ ns) is used to suppress electronic noise and energy deposits unrelated to the event.

The final state of interest is studied through the decay chain $J/\psi \rightarrow \gamma\eta', \eta' \rightarrow e^+e^-\omega, \omega \rightarrow \pi^+\pi^-\pi^0, \pi^0 \rightarrow \gamma\gamma$, and candidate events are required to have four good charged tracks with a net charge of zero and at least three photons. In the two-body decay of $J/\psi \rightarrow \gamma\eta'$, the radiative photon carries a unique energy of 1.4 GeV. Hence, to suppress background events, the most energetic photon is required to have an energy greater than 1 GeV. The remaining two photons are used to form π^0 candidates. The ω candidates are reconstructed by combining two oppositely charged pion tracks with the π^0 , and η' candidates are formed by combining the pair of e^+e^- with the ω .

The combined information of the specific ionization energy loss (dE/dx) measurements in the MDC and the flight time measured in the TOF is used to form particle identification (PID) confidence levels for the e and π hypotheses. To select candidate events, the combination with the smallest χ_{4C+PID}^2 is retained [5]. Here, $\chi_{4C+PID}^2 = \chi_{4C}^2 + \sum_{i=1}^4 \chi_{PID}^2(i)$ is the sum of the chi-squares from the four-constraint (4C) kinematic fit and PID, where i denotes the index of the four charged tracks used to form an η' candidate. The combination with $\chi_{4C+PID}^2 < 70$ is kept as an $e^+e^-\pi^+\pi^-\gamma\gamma\gamma$ candidate. To reject possible backgrounds with mis-identification between e and π , a 4C kinematic fit is performed under the hypotheses $J/\psi \rightarrow \pi^+\pi^-\pi^+\pi^-\gamma\gamma\gamma$. The events with a χ_{4C}^2 value for the signal hypothesis larger than that for the background hypothesis are discarded. The selected photon with maximum energy is taken as the radiative photon. The other two photons are further required to be consistent with a π^0 candidate, $|M(\gamma\gamma) - M(\pi^0)| < 0.015 \text{ GeV}/c^2$, where $M(\pi^0)$ is the π^0 nominal mass [16].

The primary peaking background comes from $J/\psi \rightarrow \gamma\eta', \eta' \rightarrow \gamma\omega, \omega \rightarrow \pi^+\pi^-\pi^0, \pi^0 \rightarrow \gamma\gamma$ events, where a photon converts to an e^+e^- pair at the beam pipe or the inner wall of the MDC. For such conversion backgrounds, the invariant mass of the e^+e^- pair, $M(e^+e^-)$, is expected to be close to zero. However, since the default BESIII tracking algorithm assumes the interaction point as the common origin of all tracks, the directions of tracks originating elsewhere are mis-reconstructed. As a result, the conversion pair acquires an artificial opening angle, leading to a reconstructed invariant mass larger than the true value. Therefore, the conversion background appears as a pronounced peak at about $0.015 \text{ GeV}/c^2$ in the $M(e^+e^-)$ distribution, as shown in Fig. 1(a). The distribution of the distance from the reconstructed vertex of an e^+e^- pair to the z axis, R_{xy} [22], is shown in Fig. 1(b). The peaks around $R_{xy} = 3.5 \text{ cm}$ and $R_{xy} = 6.5 \text{ cm}$ correspond to the position of the beam pipe and the inner wall of the MDC, respectively. These structures are characteristic of photon conversion backgrounds.

Events with $R_{xy} < 2 \text{ cm}$ are retained. For events with $R_{xy} \geq 2 \text{ cm}$, those satisfying both $\cos\theta_{eg} > 0$ and $-1.0 < \Delta_{xy} < 0.8 \text{ cm}$ are excluded as shown in Fig. 2(a), while the others are retained to improve statistics. Here, $\cos\theta_{eg}$ is defined as the cosine of the angle between the

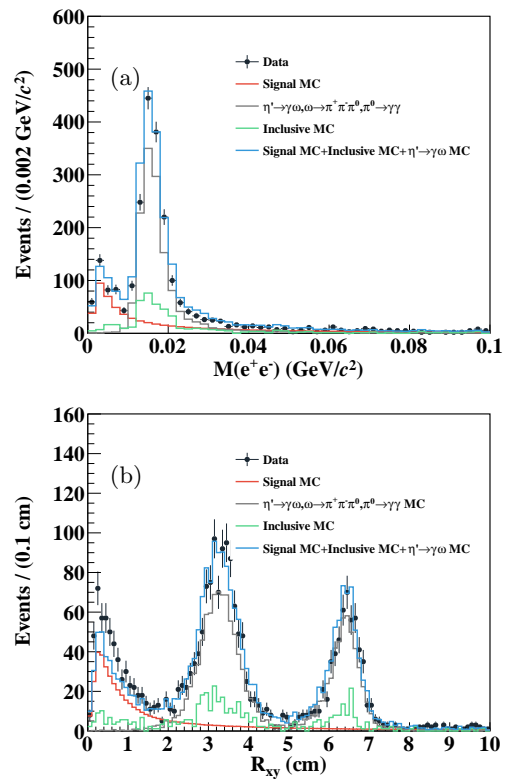


FIG. 1. The distributions of (a) $M(e^+e^-)$ and (b) the transverse distance R_{xy} of the e^+e^- vertex from the interaction point. The dots with error bars represent the data, the red line is the simulated signal shape, the gray line is the $J/\psi \rightarrow \gamma\eta', \eta' \rightarrow \gamma\omega, \omega \rightarrow \pi^+\pi^-\pi^0, \pi^0 \rightarrow \gamma\gamma$ MC shape, the green line denotes the background from the inclusive MC sample, and the blue line is the sum of all components.

momentum of the e^+e^- pair and the direction from the interaction point to the conversion point of the virtual photon $\gamma^* \rightarrow e^+e^-$. The electron and positron tracks project to two circles in the xy plane, and Δ_{xy} is the distance between the intersections of these two circles along the line connecting their centers [22]. The distributions of Δ_{xy} versus $\cos\theta_{eg}$ for the simulated signal and background MC samples are displayed in Fig. 2.

To suppress potential background events from the $\pi^0 \rightarrow \gamma e^+e^-$ decay, we require events to satisfy $|M(\gamma_1\gamma_2) - M(\pi^0)| < |M(\gamma_1 e^+e^-) - M(\pi^0)|$, $|M(\gamma_1\gamma_2) - M(\pi^0)| < |M(\gamma_2 e^+e^-) - M(\pi^0)|$. Additionally, events with $0.52 < M(\gamma_3 e^+e^-) < 0.58 \text{ GeV}/c^2$ are vetoed to suppress the background from the $\eta \rightarrow \gamma e^+e^-$ process. Here, γ_1 , and γ_2 correspond to the two photons from the π^0 decay, while γ_3 denotes the radiative photon from the $\eta \rightarrow \gamma e^+e^-$ decay. The distributions of the invariant masses of $\gamma_1 e^+e^-$, $\gamma_2 e^+e^-$ and $\gamma_3 e^+e^-$ are shown in Fig. 3. To further suppress the potential background from $J/\psi \rightarrow \gamma\eta', \eta' \rightarrow \pi^+\pi^-\eta, \eta \rightarrow \gamma e^+e^-$, events with $M(\gamma_1 e^+e^-) > 0.5 \text{ GeV}/c^2$ are rejected, as shown in Fig. 3(a).

The distribution of $M(\pi^+\pi^-\pi^0 e^+e^-)$ versus

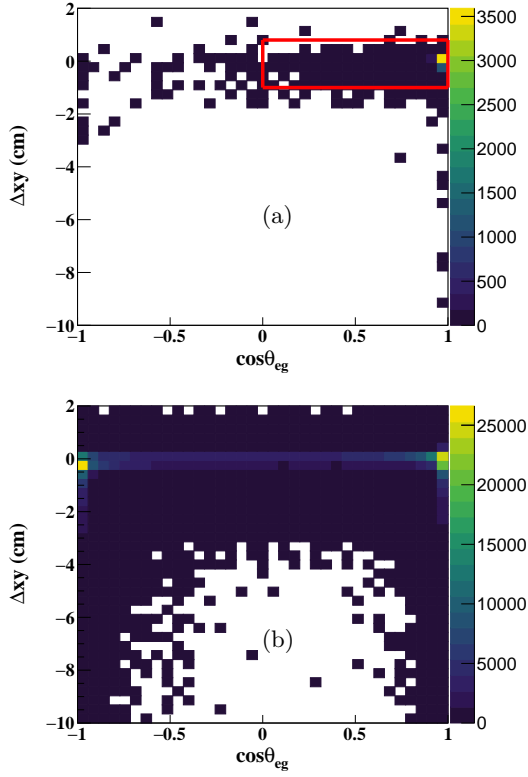


FIG. 2. The distributions of Δ_{xy} versus $\cos\theta_{eg}$ for the MC events of (a) the background $J/\psi \rightarrow \gamma\eta', \eta' \rightarrow \gamma\omega, \omega \rightarrow \pi^+\pi^-\pi^0, \pi^0 \rightarrow \gamma\gamma$ and (b) the signal process. Events located in the red rectangle are rejected.

$M(\pi^+\pi^-\pi^0)$ is shown in Fig. 4(a), where a significant background contribution is observed. Based on the study of the inclusive MC sample, the dominant contribution is from the process $\eta' \rightarrow \eta\pi^+\pi^-$, $\eta \rightarrow \pi^+\pi^-\pi^0$, as indicated in Fig. 4(b). To suppress this background, the invariant mass $M(\pi^+\pi^-\pi^0e^+e^-)$ is required to be between 0.90 GeV/ c^2 and 1.02 GeV/ c^2 .

To investigate possible background contributions, the same selection criteria are applied to the inclusive MC sample of 10 billion J/ψ events. No significant peaking background is observed in the distribution of $M(\pi^+\pi^-\pi^0e^+e^-) - M(\pi^+\pi^-\pi^0)$.

An off-resonance data sample of 167.06 pb $^{-1}$ taken at $\sqrt{s} = 3.08$ GeV is employed to estimate the possible background contribution from the continuum process. After applying the same selection criteria, no event survives. Therefore, the continuum background is neglected.

IV. BRANCHING FRACTION MEASUREMENT

To further exclude the impact of peaking backgrounds on the signal extraction, the number of signal events is determined by fitting the distribution of $M(\pi^+\pi^-\pi^0e^+e^-) - M(\pi^+\pi^-\pi^0)$, which effectively suppress η' or ω peaking backgrounds by rendering them

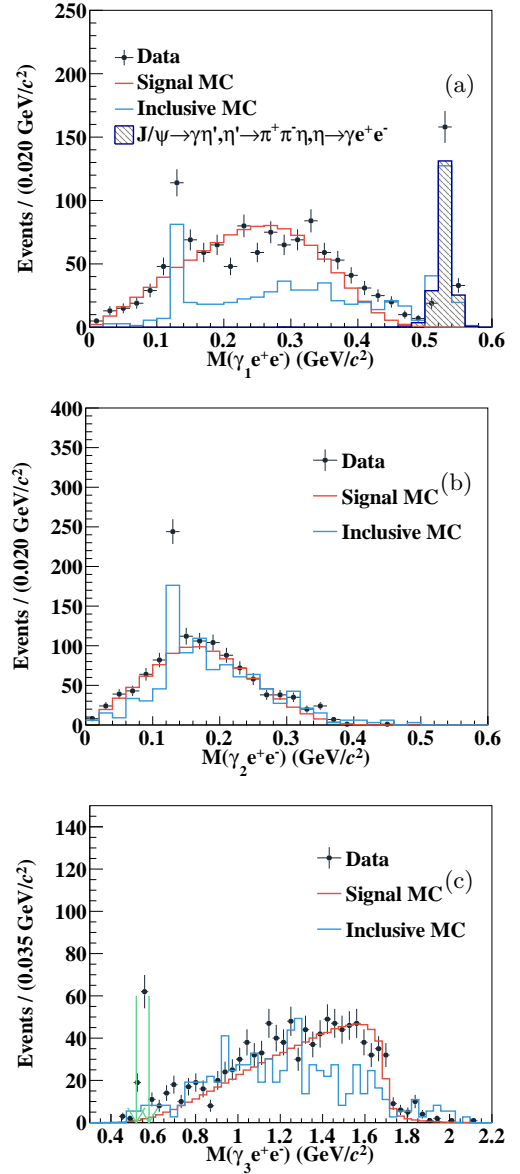


FIG. 3. The distributions of (a) $M(\gamma_1e^+e^-)$, (b) $M(\gamma_2e^+e^-)$ and (c) $M(\gamma_3e^+e^-)$. The dots with error bars represent data, the red line represents the signal MC sample, the blue line represents the inclusive MC sample, and the gray histogram represents the background from $J/\psi \rightarrow \gamma\eta', \eta' \rightarrow \pi^+\pi^-\eta, \eta \rightarrow \gamma e^+e^-$. The background region for $\eta \rightarrow \gamma e^+e^-$ is indicated by the green arrows in panel (c).

smoother. To extract the signal yield of $\eta' \rightarrow e^+e^-\omega$, an unbinned maximum-likelihood fit is performed to the distribution of $M(\pi^+\pi^-\pi^0e^+e^-) - M(\pi^+\pi^-\pi^0)$. The signal probability density function is modeled using the shape obtained from the signal MC simulation. Since the decay $\eta' \rightarrow \gamma\omega$ is not included in the inclusive MC sample, exclusive MC samples are generated for $J/\psi \rightarrow \gamma\eta', \eta' \rightarrow \gamma\omega, \omega \rightarrow \pi^+\pi^-\pi^0, \pi^0 \rightarrow \gamma e^+e^-$. Accordingly, the non-peaking background is described by the combined shape from the inclusive MC sample and the exclusive

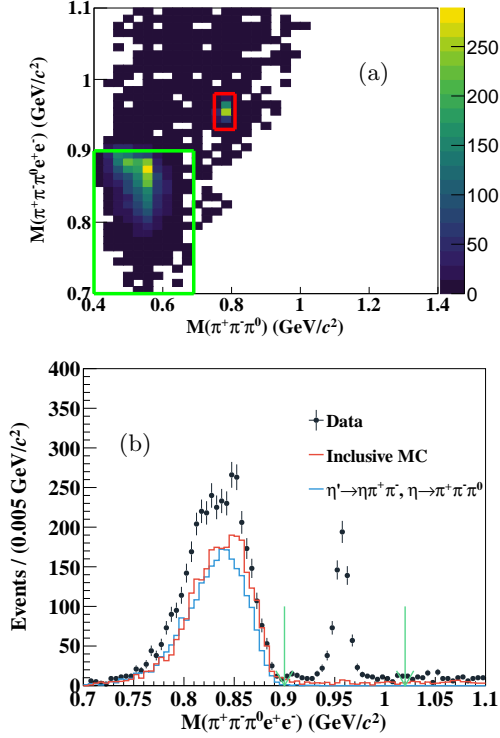


FIG. 4. (a) The distribution of $M(\pi^+\pi^-\pi^0e^+e^-)$ versus $M(\pi^+\pi^-\pi^0)$ for data. The region for the background from $\eta' \rightarrow \eta\pi^+\pi^-$, $\eta \rightarrow \pi^+\pi^-\pi^0$ is indicated by the green square and the signal region is indicated by the red square. (b) The distribution of $M(\pi^+\pi^-\pi^0e^+e^-)$. The dots with error bars represent data, the red line represents the inclusive MC sample, and the blue line represents the background from $\eta' \rightarrow \eta\pi^+\pi^-$, $\eta \rightarrow \pi^+\pi^-\pi^0$. The η' signal region is shown in the green arrows.

MC sample of $J/\psi \rightarrow \gamma\eta'$, $\eta' \rightarrow \gamma\omega$, $\omega \rightarrow \pi^+\pi^-\pi^0$, $\pi^0 \rightarrow \gamma e^+e^-$. The peaking background from photon conversion events in $J/\psi \rightarrow \gamma\eta'$, $\eta' \rightarrow \gamma\omega$, $\omega \rightarrow \pi^+\pi^-\pi^0$, $\pi^0 \rightarrow \gamma\gamma$ process is modeled using the corresponding MC shape. The fit yields $N_{\text{sig}} = 609.1 \pm 27.7$ signal events, as shown in Fig. 5. The BF of $\eta' \rightarrow e^+e^-\omega$ is determined as

$$\mathcal{B}(\eta' \rightarrow e^+e^-\omega) = \frac{N_{\text{sig}}}{N_{J/\psi} \cdot \mathcal{B}_{\text{sub}} \cdot \epsilon}, \quad (5)$$

where $N_{J/\psi}$ is the total number of J/ψ events in data, $\epsilon = 7.30\%$ is the detection efficiency, and \mathcal{B}_{sub} denotes the product BFs $\mathcal{B}(J/\psi \rightarrow \gamma\eta') \cdot \mathcal{B}(\omega \rightarrow \pi^+\pi^-\pi^0) \cdot \mathcal{B}(\pi^0 \rightarrow \gamma\gamma)$, with BFs quoted from the PDG [16]. The BF of $\eta' \rightarrow e^+e^-\omega$ is calculated to be $(1.79 \pm 0.09) \times 10^{-4}$, where the uncertainty is statistical only.

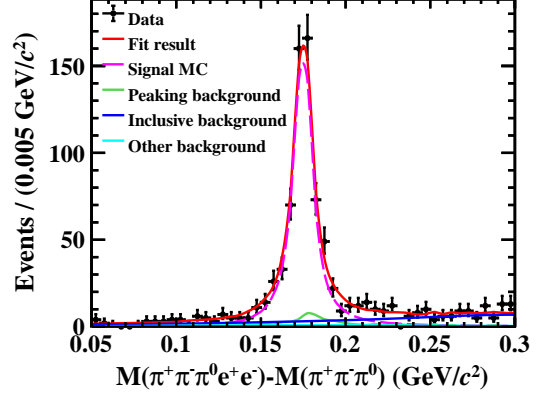


FIG. 5. The fit to the distribution of $M(\pi^+\pi^-\pi^0e^+e^-) - M(\pi^+\pi^-\pi^0)$. The dots with error bars represent the data, the red line represents the total fit result and the pink line represents the signal MC sample, the green line represents the peaking background from $J/\psi \rightarrow \gamma\eta'$, $\eta' \rightarrow \gamma\omega$, $\omega \rightarrow \pi^+\pi^-\pi^0$, $\pi^0 \rightarrow \gamma\gamma$, the blue line represents the background from the inclusive MC sample and the cyan line represents the background from $J/\psi \rightarrow \gamma\eta'$, $\eta' \rightarrow \gamma\omega$, $\omega \rightarrow \pi^+\pi^-\pi^0$, $\pi^0 \rightarrow \gamma e^+e^-$.

V. TRANSITION FORM FACTOR MEASUREMENT

To extract the TFF, a cleaner data sample is required. The signal region is further refined as $M(\pi^+\pi^-\pi^0e^+e^-) \in [0.94, 0.98] \text{ GeV}/c^2$ and $M(\pi^+\pi^-\pi^0e^+e^-) - M(\pi^+\pi^-\pi^0) \in [0.14, 0.20] \text{ GeV}/c^2$, which enhances the signal purity. With all the selection criteria applied, 586 events are retained for the TFF analysis. The distribution of $M(\pi^+\pi^-\pi^0e^+e^-)$ versus $M(\pi^+\pi^-\pi^0e^+e^-) - M(\pi^+\pi^-\pi^0)$ is shown in Fig. 6. Background contributions are estimated using the inclusive and exclusive MC samples.

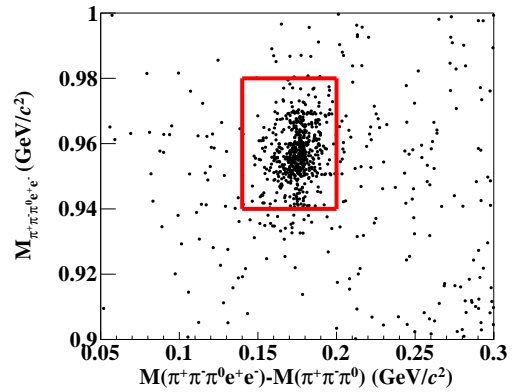


FIG. 6. The distribution of $M(\pi^+\pi^-\pi^0e^+e^-)$ versus $M(\pi^+\pi^-\pi^0e^+e^-) - M(\pi^+\pi^-\pi^0)$. The signal region for the TFF measurement is shown in the red square.

The TFF of the η' is extracted by performing an unbinned maximum-likelihood fit on the e^+e^- invariant mass spectrum of the selected $\eta' \rightarrow \omega e^+e^-$ candidates. The likelihood function is defined as

$$\mathcal{L} = \prod_{i=1}^N P(\xi_i), \quad (6)$$

where N is the number of observed events, and ξ_i represents the set of four-momenta of the final-state particle for the i -th event. The probability ($P(\xi_i)$) for observing the i -th event is given by

$$P(\xi_i) = \frac{\omega(\xi_i)\epsilon(\xi_i)}{\int d\xi \omega(\xi)\epsilon(\xi)}, \quad (7)$$

where $\omega(\xi_i) \equiv (d\sigma/d\phi)_i$ represents the differential cross section, $\epsilon(\xi_i)$ the detection efficiency, and $\int d\xi \omega(\xi)\epsilon(\xi)$ represents the measured total cross section.

In this analysis, the squared amplitude for the decay $\eta' \rightarrow e^+e^-\omega$ is given by Eq. 1.

In the log-likelihood calculation, background events are assigned negative weights, i.e.

$$-\ln\mathcal{L} = \omega' \left[-\left(\sum_i^{N_{\text{data}}} \ln \mathcal{L}_{\text{data}} - \sum_j^{N_{\text{bkg}}} \omega_j \cdot \ln \mathcal{L}_{\text{bkg}} \right) \right], \quad (8)$$

where i runs over all accepted data events, and j runs over the considered background events. The estimated number of background events, listed in Table I, are fixed according to their normalization to the data luminosity. To obtain an unbiased uncertainty, a normalization factor derived from Ref. [23] is defined as

$$\omega' = \frac{N_{\text{data}} - \sum_j N_{\text{bkg}}^j \omega_j}{N_{\text{data}} + \sum_j N_{\text{bkg}}^j \omega_j^2}, \quad (9)$$

where N_{data} and N_{bkg}^j are the numbers of data events and the j -th background component, respectively, and ω_j is the corresponding background weight.

TABLE I. The estimated numbers of background events N_{bkg} for different background components.

Component	N_{bkg}
$\eta' \rightarrow \gamma\omega, \omega \rightarrow \pi^+\pi^-\pi^0, \pi^0 \rightarrow \gamma\gamma$	32.8
$\eta' \rightarrow \gamma\omega, \omega \rightarrow \pi^+\pi^-\pi^0, \pi^0 \rightarrow \gamma e^+e^-$	8.4
Inclusive background	18.0
Total	59.2

The fit yields $\Lambda^{-1} = (2.92 \pm 0.83) \text{ GeV}^{-1}$, where the uncertainty is statistical only. A comparison between the fit results and the e^+e^- invariant mass distribution of the data is presented in Fig. 7.

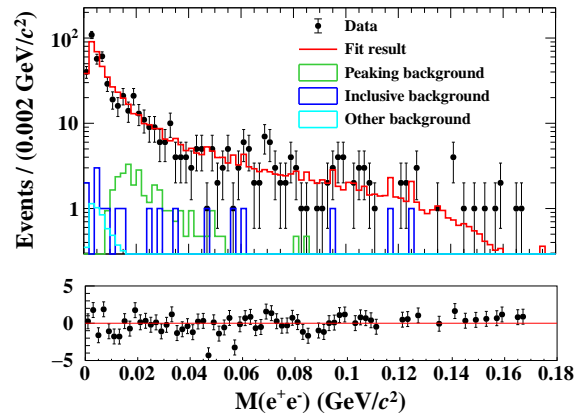


FIG. 7. The e^+e^- invariant mass distribution and the fit result of the TFF. The dots with error bars represent the data, the red line represents the total fit result, the green histogram represents the peaking background from $J/\psi \rightarrow \gamma\eta', \eta' \rightarrow \gamma\omega, \omega \rightarrow \pi^+\pi^-\pi^0, \pi^0 \rightarrow \gamma\gamma$, the blue histogram represents the background from the inclusive MC sample and the cyan histogram represents the background from $J/\psi \rightarrow \gamma\eta', \eta' \rightarrow \gamma\omega, \omega \rightarrow \pi^+\pi^-\pi^0, \pi^0 \rightarrow \gamma e^+e^-$.

VI. SYSTEMATIC UNCERTAINTIES

The systematic uncertainties of the TFF measurement originate mainly from the MDC tracking and PID of charged particles, the photon detection, the kinematic fit, the background suppression criteria, and the estimation of background contamination. The BF measurement shares these uncertainties and suffers from additional effects from the mass fit range, the total number of J/ψ events, and the external BFs from the PDG [16]. All systematic uncertainties are assumed to be independent and added in quadrature. The individual contributions are summarized in Table II and are described in detail below.

- MDC tracking and PID: The efficiency differences of data and MC simulation for pion MDC tracking and PID are studied using the control sample of $J/\psi \rightarrow \pi^+\pi^-\pi^0$ [24]. The tracking efficiencies for electrons are obtained with the control sample of radiative Bhabha scattering $e^+e^- \rightarrow e^+e^-\Gamma_{\text{ISR}}$ [25] (including $J/\psi \rightarrow e^+e^-\gamma_{\text{FSR}}$) at $\sqrt{s} = 3.097 \text{ GeV}$. The differences between data and MC simulation are parametrized as the momentum- and polar-angle-dependent correction factors, which are applied according to the event weights in the signal MC sample. The weighted uncertainties are taken as the systematic uncertainties.
- Photon detection: The systematic uncertainty associated with photon reconstruction is obtained with the control sample of $e^+e^- \rightarrow \mu^+\mu^-\gamma_{\text{ISR}}$. The photon detection efficiencies are determined

as two-dimensional functions of the photon energy and polar angle. For the TFF measurement, the efficiency of signal MC simulation is corrected by the ratio $\epsilon_{\text{data}}/\epsilon_{\text{MC}}$, where ϵ_{data} and ϵ_{MC} are the 2D efficiency obtained from the control sample, respectively. The resulting variation in the extracted TFF is assigned as the associated systematic uncertainty. For the BF measurement, the systematic uncertainties are weighted according to the photon energy and angular distributions in data and MC simulation, and are taken as the corresponding uncertainties.

- Kinematic fit: To investigate the systematic uncertainty associated with the kinematic fit, the track helix parameter correction method [26] is used. The difference in detection efficiencies between samples with and without the helix parameter correction is taken as the systematic uncertainty.
- Photon conversion veto: The systematic uncertainty due to the photon conversion veto is estimated by varying the nominal criterion to $R_{xy} > 1.9$ cm or $R_{xy} > 2.1$ cm. The resulting change in the final results is assigned as the associated uncertainty.
- π^0 or η' mass window: The systematic uncertainty arising from the π^0 or η' mass window is determined by varying the corresponding mass window by one standard deviation. The resulting differences of the BF and the TFF are taken as the uncertainty.
- $M(\gamma_{1/3}e^+e^-)$ range: The uncertainty arising from the $M(\gamma_{1/3}e^+e^-)$ range is determined by changing the $M(\gamma_{1/3}e^+e^-)$ range by 0.02 GeV/ c^2 and 0.008 GeV/ c^2 , respectively. The corresponding changes in the BF and the TFF are taken as the systematic uncertainties.
- Peaking background: The peaking background contribution is estimated using the BFs of $J/\psi \rightarrow \gamma\eta'$, $\eta' \rightarrow \gamma\omega$, $\omega \rightarrow \pi^+\pi^-\pi^0$, $\pi^0 \rightarrow \gamma\gamma$ quoted from the PDG [16]. By varying the BFs within their $\pm 1\sigma$ of uncertainties, the change in the final result is taken as the corresponding uncertainty.
- Non-peaking background: The non-peaking background contribution is estimated using the BFs of $J/\psi \rightarrow \gamma\eta'$, $\eta' \rightarrow \gamma\omega$, $\omega \rightarrow \pi^+\pi^-\pi^0$, $\pi^0 \rightarrow \gamma e^+e^-$ quoted from the PDG [16]. The number of background events is varied by $\pm 1\sigma$, and the resulting change in the final results is taken as the systematic uncertainty.
- Fit range: The uncertainty arising from the fit range in the BF is determined to be 2.2% by changing the fit range by ± 0.02 GeV/ c^2 .
- Number of J/ψ events: The number of J/ψ events is determined to be $(10087 \pm 44) \times 10^6$ from the

inclusive hadron events, corresponding to a relative uncertainty of 0.4% [6].

- Intermediate decay: The uncertainties of the quoted BFs for the intermediate decays $J/\psi \rightarrow \gamma\eta'$, $\omega\pi^+\pi^-\pi^0$, and $\pi^0 \rightarrow \gamma\gamma$ are taken from the PDG [16].

TABLE II. Summary of the systematic uncertainties for BF and TFF measurements (in percent).

Source	BF	TFF
MDC tracking	5.7	0.7
PID	1.1	0.3
Photon detection	1.2	0.3
Kinematic fit	0.6	1.0
Photon conversion veto	0.6	1.4
π^0 mass window	0.6	3.1
η' mass window	1.1	3.1
$M(\gamma_1 e^+ e^-)$ range	0.1	0.3
$M(\gamma_3 e^+ e^-)$ range	0.6	0.7
Peaking background	1.1	1.0
Non-peaking background	0.6	0.7
Fit range	2.2	-
Number of J/ψ events	0.4	-
Intermediate decays	1.4	-
Total	6.8	5.0

VII. SUMMARY

Based on a sample of $(10087 \pm 44) \times 10^6$ J/ψ events collected with the BESIII detector, the decay $\eta' \rightarrow e^+e^-\omega$ is studied. The BF is determined to be $\mathcal{B}(\eta' \rightarrow e^+e^-\omega) = (1.79 \pm 0.09 \text{ (stat.)} \pm 0.12 \text{ (syst.)}) \times 10^{-4}$. This result is consistent with the previous measurement and theoretical predictions, and improves the experimental precision by a factor of 2.7, as shown in Fig. 8.

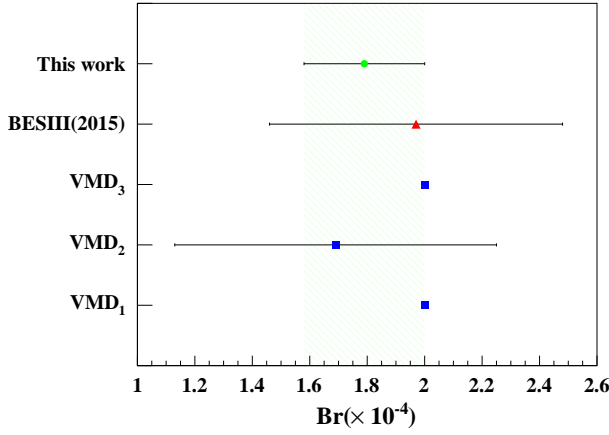


FIG. 8. The BF's of the $\eta' \rightarrow e^+e^-\omega$ from different theoretical predictions [4, 27, 28] (blue squares), the previous experiments [5] (red triangle), and the results of this work (green squares and green dot).

The transition form factor parameter Λ^{-1} of $\eta' \rightarrow e^+e^-\omega$ is measured for the first time to be $(2.92 \pm 0.83 \text{ (stat.)} \pm 0.15 \text{ (syst.)}) \text{ GeV}^{-1}$. This parameter provides important input for phenomenological studies of η' electromagnetic transitions. Since the present measurement is limited by statistics, a larger η' data sample is needed to further improve the precision in the future.

ACKNOWLEDGMENTS

The BESIII Collaboration thanks the staff of BEPCII [29] and the IHEP computing center for their

strong support. This work is supported in part by National Key R&D Program of China under Contracts No. 2025YFA1613900, No. 2023YFA1606000, No. 2023YFA1606704; National Natural Science Foundation of China (NSFC) under Contracts No. 12225509, No. 12465015, No. 12575087, No. 11635010, No. 11935015, No. 11935016, No. 11935018, No. 12025502, No. 12035009, No. 12035013, No. 12061131003, No. 12192260, No. 12192261, No. 12192262, No. 12192263, No. 12192264, No. 12192265, No. 12221005, No. 12235017, No. 12342502, No. 12361141819; the Chinese Academy of Sciences (CAS) Large-Scale Scientific Facility Program; the Strategic Priority Research Program of Chinese Academy of Sciences under Contract No. XDA0480600; CAS under Contract No. YSBR-101; 100 Talents Program of CAS; The Institute of Nuclear and Particle Physics (INPAC) and Shanghai Key Laboratory for Particle Physics and Cosmology; ERC under Contract No. 758462; German Research Foundation DFG under Contract No. FOR5327; Istituto Nazionale di Fisica Nucleare, Italy; Knut and Alice Wallenberg Foundation under Contracts No. 2021.0174, No. 2021.0299, No. 2023.0315; Ministry of Development of Turkey under Contract No. DPT2006K-120470; National Research Foundation of Korea under Contract No. NRF-2022R1A2C1092335; National Science and Technology fund of Mongolia; Polish National Science Centre under Contract No. 2024/53/B/ST2/00975; STFC (United Kingdom); Swedish Research Council under Contract No. 2019.04595; U. S. Department of Energy under Contract No. DE-FG02-05ER41374

-
- [1] G. R. Kalbfleisch *et al.*, *Phys. Rev. Lett.* **12**, 527 (1964).
 - [2] M. Goldberg *et al.*, *Phys. Rev. Lett.* **12**, 546 (1964).
 - [3] M. Ablikim *et al.* (BESIII Collaboration), *Phys. Rev. D* **87**, 092011 (2013).
 - [4] A. Faessler, C. Fuchs, and M. I. Krivoruchenko, *Phys. Rev. C* **61**, 035206 (2000).
 - [5] M. Ablikim *et al.* (BESIII Collaboration), *Phys. Rev. D* **92**, 051101 (2015).
 - [6] M. Ablikim *et al.* (BESIII Collaboration), *Chin. Phys. C* **46**, 074001 (2022).
 - [7] M. Ablikim *et al.* (BESIII Collaboration), *Nucl. Instrum. Meth. A* **614**, 345 (2010).
 - [8] C. H. Yu *et al.*, in *Proceedings of IPAC2016* (JACoW, Busan, Korea, 2016).
 - [9] M. Ablikim *et al.* (BESIII Collaboration), *Chin. Phys. C* **44**, 040001 (2020).
 - [10] P. Cao *et al.*, *Nucl. Instrum. Meth. A* **953**, 163053 (2020).
 - [11] S. Agostinelli *et al.* (GEANT4), *Nucl. Instrum. Meth. A* **506**, 250 (2003).
 - [12] S. Jadach, B. F. L. Ward, and Z. Was, *Phys. Rev. D* **63**, 113009 (2001).
 - [13] S. Jadach, B. F. L. Ward, and Z. Was, *Comput. Phys. Commun.* **130**, 260 (2000).
 - [14] D. J. Lange, *Nucl. Instrum. Meth. A* **462**, 152 (2001).
 - [15] R. G. Ping, *Chin. Phys. C* **32**, 599 (2008).
 - [16] S. Navas *et al.* (Particle Data Group), *Phys. Rev. D* **110**, 030001 (2024).
 - [17] J. C. Chen, G. S. Huang, X. R. Qi, D. H. Zhang, and Y. S. Zhu, *Phys. Rev. D* **62**, 034003 (2000).
 - [18] R. L. Yang, R. G. Ping, and H. Chen, *Chin. Phys. Lett.* **31**, 061301 (2014).
 - [19] E. Richter-Was, *Phys. Lett. B* **303**, 163 (1993).
 - [20] N. Qin, Z. Y. Zhang, S. S. Fang, X. Zhou, L. L. Du, and H. X. Qiao, *Chin. Phys. C* **42**, 013001 (2018).
 - [21] L. G. Landsberg, *Phys. Rept.* **128**, 301 (1985).
 - [22] Z. R. Xu and K. L. He, *Phys. Rev. C* **36**, 742 (2012).
 - [23] C. Langenbruch, *Eur. Phys. J. C* **82**, 393 (2022).
 - [24] F. Liu *et al.*, *Radiat. Detect. Technol. Methods* **9**, 390 (2025).
 - [25] X. Y. Chai *et al.*, *Radiat. Detect. Technol. Methods* (2025).
 - [26] M. Ablikim *et al.* (BESIII Collaboration), *Phys. Rev. D* **87**, 012002 (2013).
 - [27] C. Terschlüsen, S. Leupold, and M. F. M. Lutz, *Eur. Phys. J. A* **48**, 190 (2012).
 - [28] Y. L. Yang, J. S. Huang, and G. R. Lu, *Chin. Phys. C*

39, 023102 (2015).

[29] <https://cstr.cn/31109.02.BEPC>.